

Organization of an axisymmetric turbulent wake in presence of a central protrusion

Gentile V., Schrijer F. F. J., Van Oudheusden B. W., Scarano F.

Delft University of Technology, Kluyverweg 2, 2629HT, Delft, The Netherlands

Abstract Stereoscopic Particle Image Velocimetry (PIV) was used to study the wake of an ogive-cylinder with after-body at a diameter-based Reynolds number $Re_D = 6.7 \cdot 10^4$. The vertical fluctuations reduced from a maximum of $0.18 U_\infty$ in absence of rear-protrusion, up to $0.12 U_\infty$ and $0.1 U_\infty$ when the main-body to after-body diameter ratio d/D was increased to 0.2 and 0.4 respectively. For $d/D = 0.2$ the trace of the backflow centroid motion reflected the occurrence of a random motion where no pattern associated with a consistent precession of the reverse flow region can be identified, whereas a preferred azimuthal direction could be detected for $d/D = 0.4$. Proper Orthogonal Decomposition showed that modes $k = 1, 2$ contribute up to 20% and 11% of the turbulent kinetic energy, for $d/D = 0.2$ and $d/D = 0.4$ respectively. For $d/D = 0.2$ the two modes were found to be paired and to feature a dipole organization which is linked to a displacement of the wake in all azimuthal directions. For $d/D = 0.4$ only the first mode exhibited such an arrangement, thus reflecting wake displacement occurring along a preferred azimuthal direction.

Introduction

The wake flow past a bluff body of revolution is typically characterized by a low-frequency unsteadiness related to the shedding of vortices within the shear layer at a non-dimensional frequency $St_D \approx 0.2$ (Fuchs et al. 1979, Dépres et al. 2004) and to the precession of the shedding angle at a non-dimensional frequency of $St_D \approx 10^{-3}$ (Rigas et al. 2014, Grandemange et al. 2014). Although such low-frequency unsteadiness are common to different bluff geometries, base modifications can significantly alter the spatial organization of the separated flow and influence its fluctuating behavior. Wolf et al. (2012) showed that for an ogive-cylinder the turbulence intensity reduces by approximately 25% in presence of a rear-protrusion. The studies of Dépres et al. (2004) indicate that an elongation of the after-body in relation to the base diameter is strongly linked to the occurrence of a solid reattachment of the shear layer, therefore affecting the overall organiza-

tion and unsteady behavior of the wake. Gentile et al. (2015a) recently discussed how the after-body diameter affects the radial velocity fluctuations as well as the non-dimensional recirculation bubble dimensions and flow topology, but did not investigate the azimuthal flow dynamics.

In the current study Stereoscopic Particle Image Velocimetry (PIV) is used in a plane perpendicular to the free stream to characterize the azimuthal wake organization. The statistical and instantaneous flow properties are characterized for different values of the main body to after-body diameter ratio d/D and Proper Orthogonal Decomposition is used to identify the large-scale velocity fluctuations dominating the near-wake dynamics.

Experimental apparatus and technique

The experiments were conducted in an open-exit low-speed wind tunnel. The model is an ogive-cylinder (Figure 1) equipped with a cylindrical after-body whose length is such to ensure solid reattachment (Dépres et al. 2004). The after-body diameter was varied in the range $d/D = d^* = \{0.2, 0.4\}$.

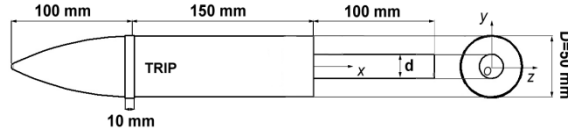


Fig. 1 Model schematic with coordinate system

The measurements were performed at a free stream velocity $U_\infty = 20$ m/s. The boundary layer over the model was tripped with a carborundum roughness strip, its thickness 5 mm upstream of separation being $\delta_{95} = 4.8$ mm. The PIV measurements were performed in planes perpendicular to the free stream flow and located at $x/D = x^* = \{0.375, 0.75\}$, corresponding to approximately 0.31 and 0.63 of the reattachment length for $d^* = 0.2$ and 0.38 and 0.75 of the reattachment length for $d^* = 0.4$ (Gentile et al. 2015a)

The flow was seeded using a SAFEX smoke generator producing a concentration of approximately 5 particles/mm³. Illumination was provided by a Quantronix Darwin Duo Nd-YLF laser. The particle images were recorded using three Photron Fast-CAM SA1.1 CMOS cameras (1024 × 1024 pixels 5400 fps, 20 μm pixel pitch). The maximum angle between the cameras was 35 degrees yielding a relative error on the out-of-plane component equal to 3 (Prasad 2000). The illumination and recording systems were synchronized by means of a LaVision High Speed Controller hosted by a PC using Davis 8.1 software.

The recorded images were pre-processed in order to attenuate the light reflections from the model surface. An iterative multi-grid cross-correlation analysis based on window deformation (Scarano and Riethmuller 2000) was used in the vector calculation. Spurious vectors were detected using the universal median filter (Westerweel and Scarano 2005). The main experimental parameters are listed in Table 1.

Table 1 Main experimental parameters

Laser Pulse separation	dt [μ s]	25
Laser sheet thickness	t [mm]	3
Field-of-view size	FOV [mm^2]	80 x 80
Optical magnification factor	M [-]	0.17
Acquisition frequency	f [kHz]	0.1
Data ensemble size	N [-]	5,000
Vector pitch	p [mm]	0.9

Flow field statistics

The mean velocity field (normalized with respect to U_∞) is presented in Figure 2 for all configurations including a truncated-base with $d^* = 0$ as a reference (see Gentile et al. 2015b for further details on the experiments).

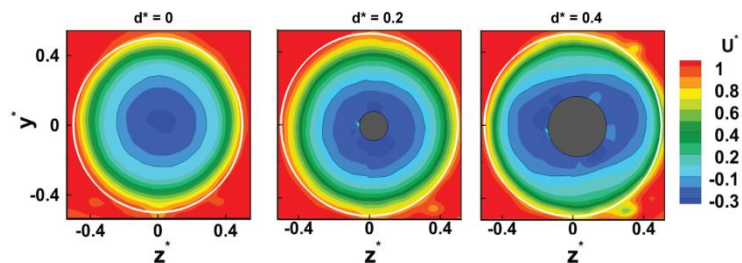


Fig. 2 Time-averaged velocity contours at $x^* = 0.75$. Solid line represents the trace of the model base

The streamwise distributions of the vertical fluctuations reported in Figure 3 (see Gentile et al. 2015a for further details on the experiments) outline a reduction of the peak values from $0.18 U_\infty$ for $d^* = 0$ to $0.12 U_\infty$ and $0.10 U_\infty$, for $d^* = 0.2$ and $d^* = 0.4$ respectively, which facts indicates a pronounced sensitivity of the separated flow towards the after-body diameter and endorses the hypothesis promoted in former investigations (Wolf et al. 2012) that the after-body tends to stabilize the unsteadiness of the separated flow.

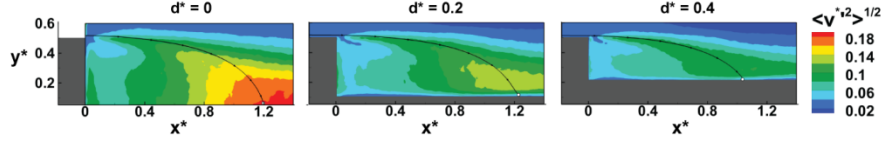


Fig. 3 Contours of the rms of the vertical velocity fluctuations at $z^* = 0$. Reattachment streamline reported as a reference

Recirculation region unsteadiness

The time variability of the recirculation region is investigated by evaluating the instantaneous backflow centroid (z_c^*, y_c^*). Figure 4 shows the coordinates of the centroid collected over an observation-time of $2,000 D/U_\infty$ (i.e. 5 s in real time) and obtained after applying a sliding average over a time-interval of $40 D/U_\infty$ (i.e. 10 raw snapshots) such to attenuate the scatter in the instantaneous data.

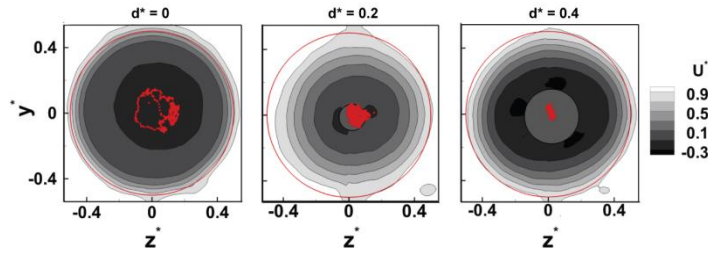


Fig. 4 Trace of backflow motion at $x^* = 0.375$. Observation-time is $2,000 D/U_\infty$. Color contours refer to the time-averaged streamwise velocity

Unlike what is observed for bluff-based geometries (Rigas et al. 2014, Grandemange et al. 2014, Gentile et al. 2015b), no consistent pattern associated with a precession about the model symmetry axis can be identified for $d^* = 0.2$. For $d^* = 0.4$ a slight preference for the backflow centroid motion is found along the y^* axis.

Proper Orthogonal Decomposition

The large-scale organization of the flow structures dominating the near-wake dynamics is characterized based on POD analysis.

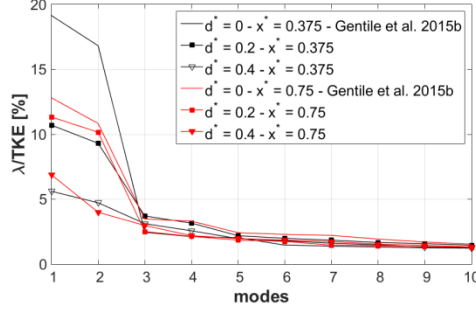


Fig. 5 Turbulent kinetic energy distribution over the first 10 modes

The POD energy spectra of Figure 5 indicate a substantial contribution of the first two POD modes ($k = 1, 2$) to the turbulent kinetic energy, thus highlighting the occurrence of large-scale fluctuations. In presence of central protrusion the energy associated with these modes increases while moving downstream, up to 20% and 11%, for $d^* = 0.2$ and $d^* = 0.4$ respectively. For $d^* = 0$ instead, it decreases moving away from the base, which difference can be mainly attributed to the smaller flow scales associated with the inner backflow dynamics.

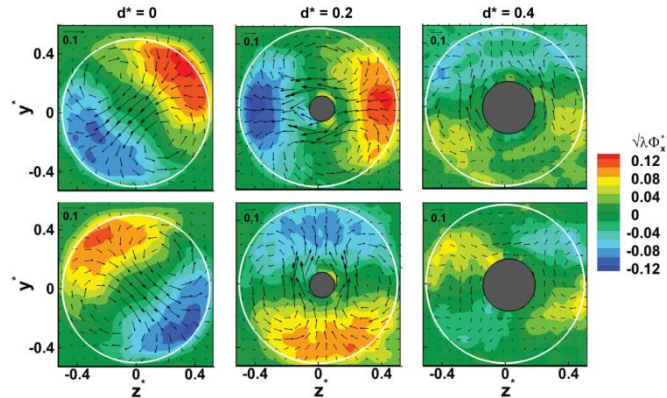


Fig. 6 Eigen-functions of $k = 1$ (left) and $k = 2$ (right) at $x^* = 0.75$. Vector arrows plotted every 4th grid point represent in-plane components $\sqrt{\lambda}\Phi_z^*$ and $\sqrt{\lambda}\Phi_y^*$

The spatial eigen-functions shown in Figure 6 outline a *dipolar* organization for $d^* = 0.2$ linked to a wake offset without any preference in the azimuthal direction. For $d^* = 0.4$ such an arrangement is preserved by mode $k = 1$ only, thus being associated with a wake displacement along a preferential azimuthal direction and being consistent with the pattern reported in Figure 4. The quadrupolar organization of mode $k = 2$ can instead be related to an *ovalization* of the wake along a preferred azimuthal direction.

Conclusions

The turbulent wake of an ogive-cylinder with after-body was studied with Stereoscopic Particle Image Velocimetry (PIV) at a diameter-based Reynolds number $Re_D = 6.7 \cdot 10^4$. Varying the after-body to main-body diameter ratio d^* showed that for $d^* = 0.4$ a rear-protrusion reduces the vertical velocity fluctuations by approximately 44% compared to a bluff-based geometry. For $d^* = 0.2$ the trace of the backflow centroid motion did not indicate any pattern associated with a consistent precession around the model symmetry axis, whereas it revealed a preferential azimuthal direction for $d^* = 0.4$.

The POD modes $k = 1, 2$ were found to capture up to 20% and 11% of the turbulent kinetic energy, for $d^* = 0.2$ and $d^* = 0.4$ respectively, being paired for $d^* \leq 0.2$. In this case the two modes were found to arrange as a dipole, being linked to a wake displacement in any azimuthal direction. For $d^* = 0.4$ instead, only mode $k = 1$ exhibited such an arrangement, reflecting a preferred azimuthal direction in the wake displacement, whereas mode $k = 2$ was found to arrange as a quadrupole being associated with ovalization of the wake.

References

- Dépres, D., Reijasse, P., and Dussauge, J. P.: Analysis of Unsteadiness in Afterbody Transonic Flows. *AIAA J* **42**(12), 2541-2550 (2004)
- Fuchs, H. V., Mercker, E., and Michel, U.: Large-scale coherent structures in the wake of axisymmetric bodies. *J Fluid Mech* **93**(1), 185-207 (1979)
- Gentile, V., Schrijer, F. F. J., Van Oudheusden, B. W., and Scarano, F.: Afterbody Effects on Axisymmetric Base Flows. In: Abstracts of the 53rd AIAA Aerospace Sciences Meeting, Kissimmee, 5-9 January 2015
- Gentile, V., Schrijer, F. F. J., Van Oudheusden, B. W., and Scarano, F.: Time-dependent behaviour of the recirculation region behind an axisymmetric bluff body. In: Abstracts of the 9th Symposium on Turbulence and Shear Flow Phenomena, Melbourne, 30 June-3 July 2015
- Grandemange, M., Gohlke, M., and Cadot, O.: Statistical axisymmetry of the turbulent sphere wake. *Exp Fluids* **55**(11), 1-11 (2014)
- Prasad, A. K.: Stereoscopic particle image velocimetry. *Exp Fluids* **29**(2), 103-116 (2000)
- Rigas, G., Oxlade, A. R., Morgans, A. S., and Morrison, J. F.: Low-dimensional dynamics of a turbulent axi-symmetric wake. *J Fluid Mech* **755**, 185-207 (2014)
- Scarano, F., and Riethmuller, M. L.: Advances in Iterative Multigrid PIV Image Processing. *Exp Fluids* **29**(1), 51-60 (2000)
- Westerweel, J., and Scarano, F.: Universal Outlier Detection for PIV Data. *Exp Fluids* **39**(1), 1096-1100 (2005)
- Wolf, C. C., Klei, C. E., Buffo, R. M., Hörnschemeyer, R., and Stumpf, E.: Comparison of Rocket Near-wakes with and without Nozzle Simulation in Subsonic Freestream Conditions. In: Abstracts of the 42nd AIAA Fluid Dynamics Conference and Exhibit, New Orleans, 25-28 June 2012